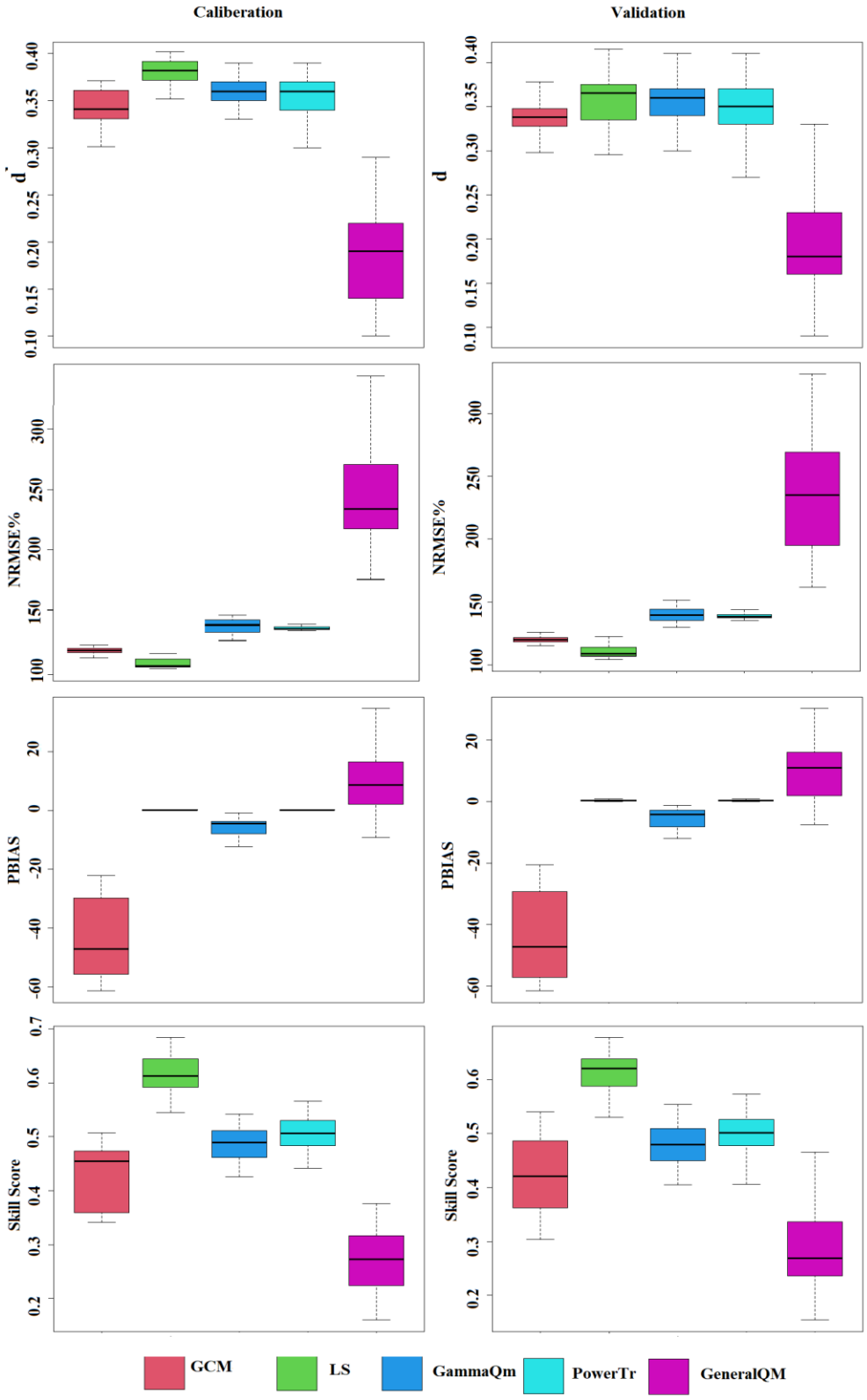

Figure S1. The statistical performance of the downscaled and raw EC-Earth-Veg GCMs for precipitation

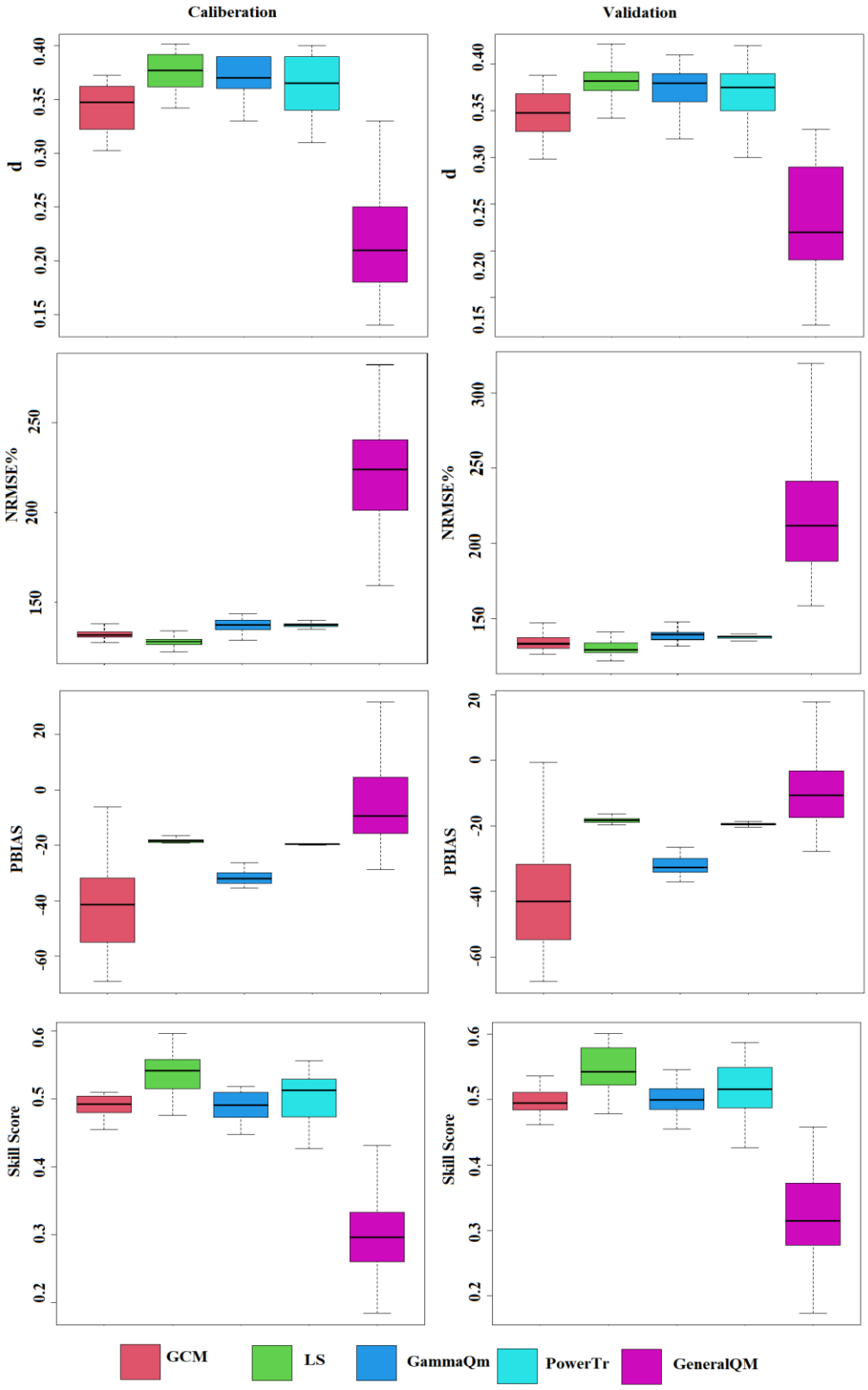

Figure S2. The statistical performance of the downscaled and raw MRI-ESM2 GCMs for precipitation

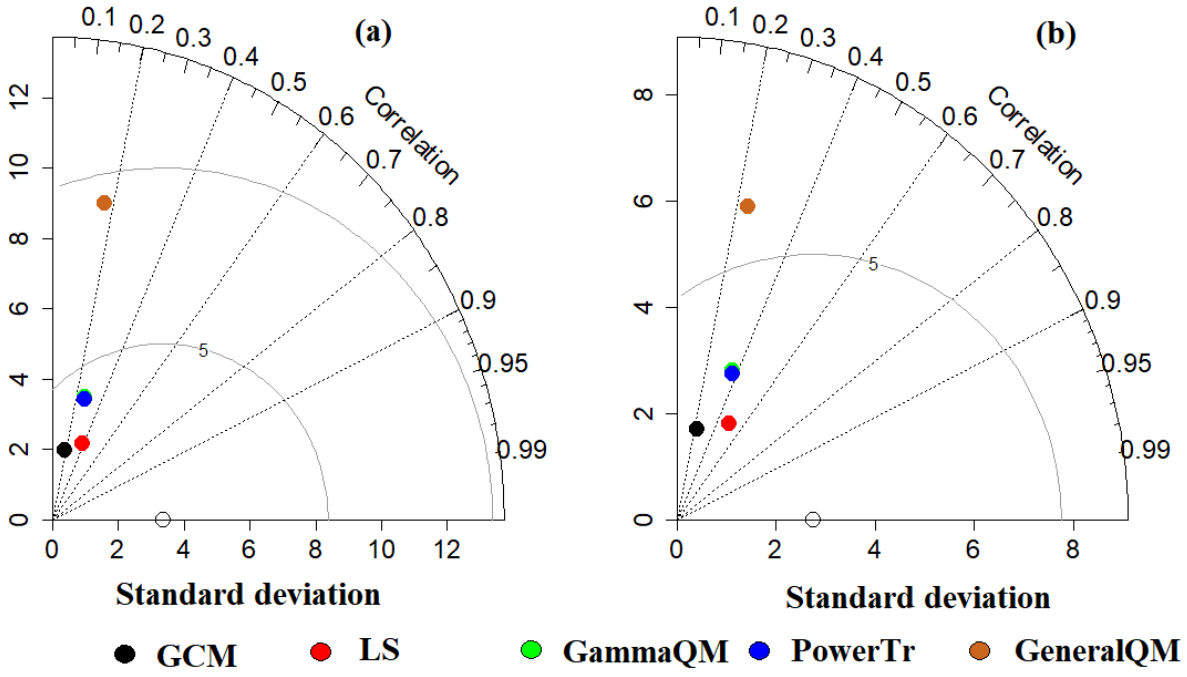

Figure S3. Taylor diagram shows bias correction methods' performance to correct EC-Earth-Veg during **(a)** cali-bration; **(b)** validation periods.

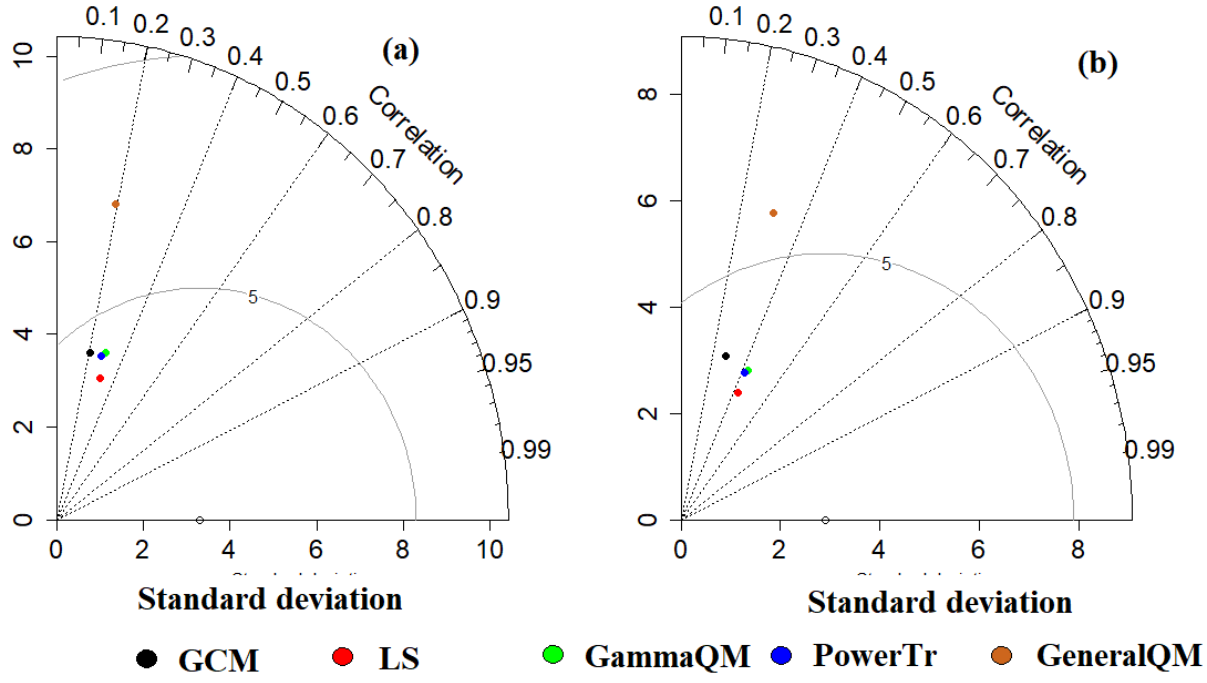

Figure S4. Taylor diagram shows bias correction methods' performance to correct MRI-ESM2 during **(a)** calibration; **(b)** validation periods.

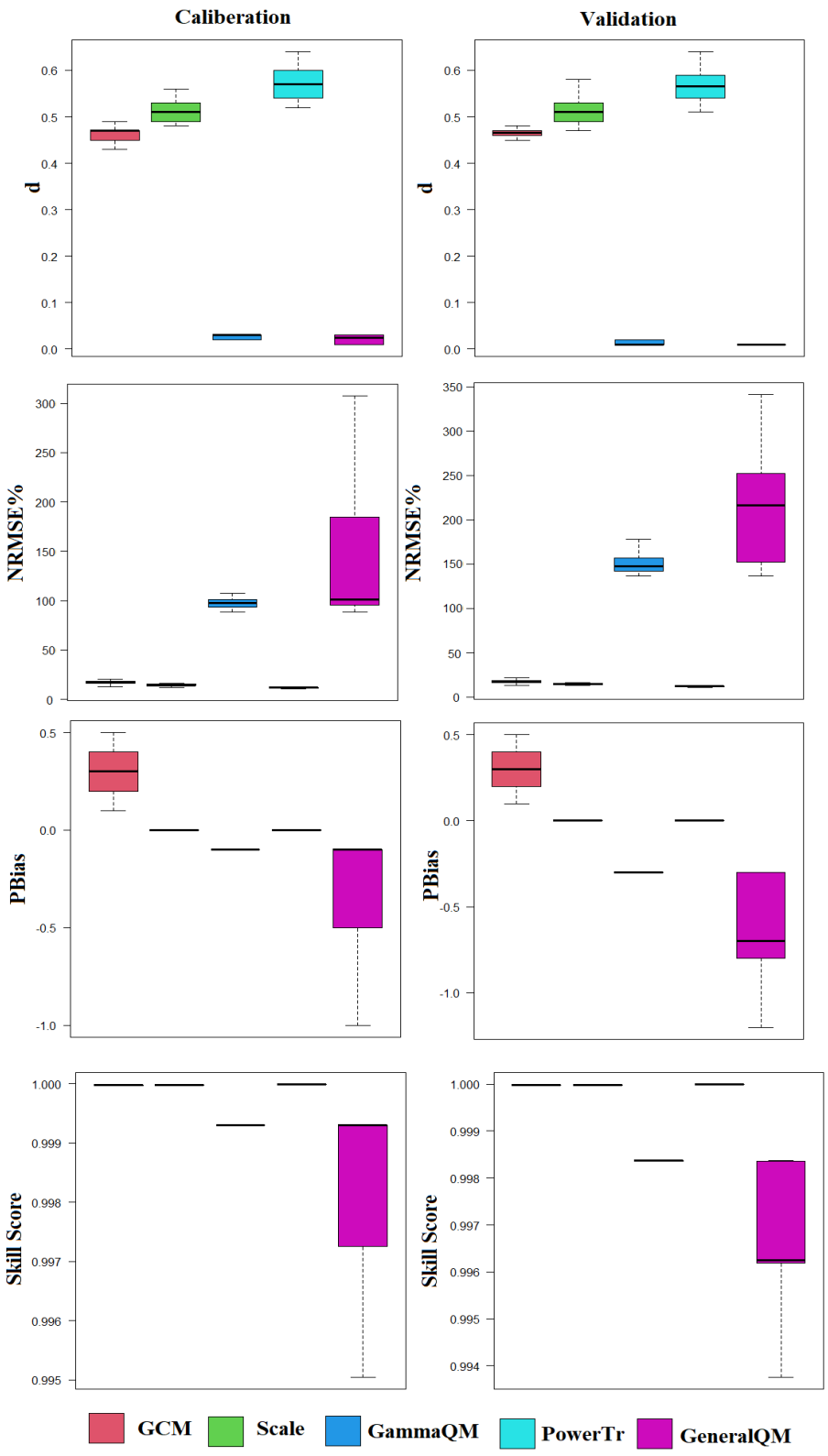

Figure S5. The statistical performance of the downscaled and raw EC-Earth-Veg GCMs for maximum temperature.

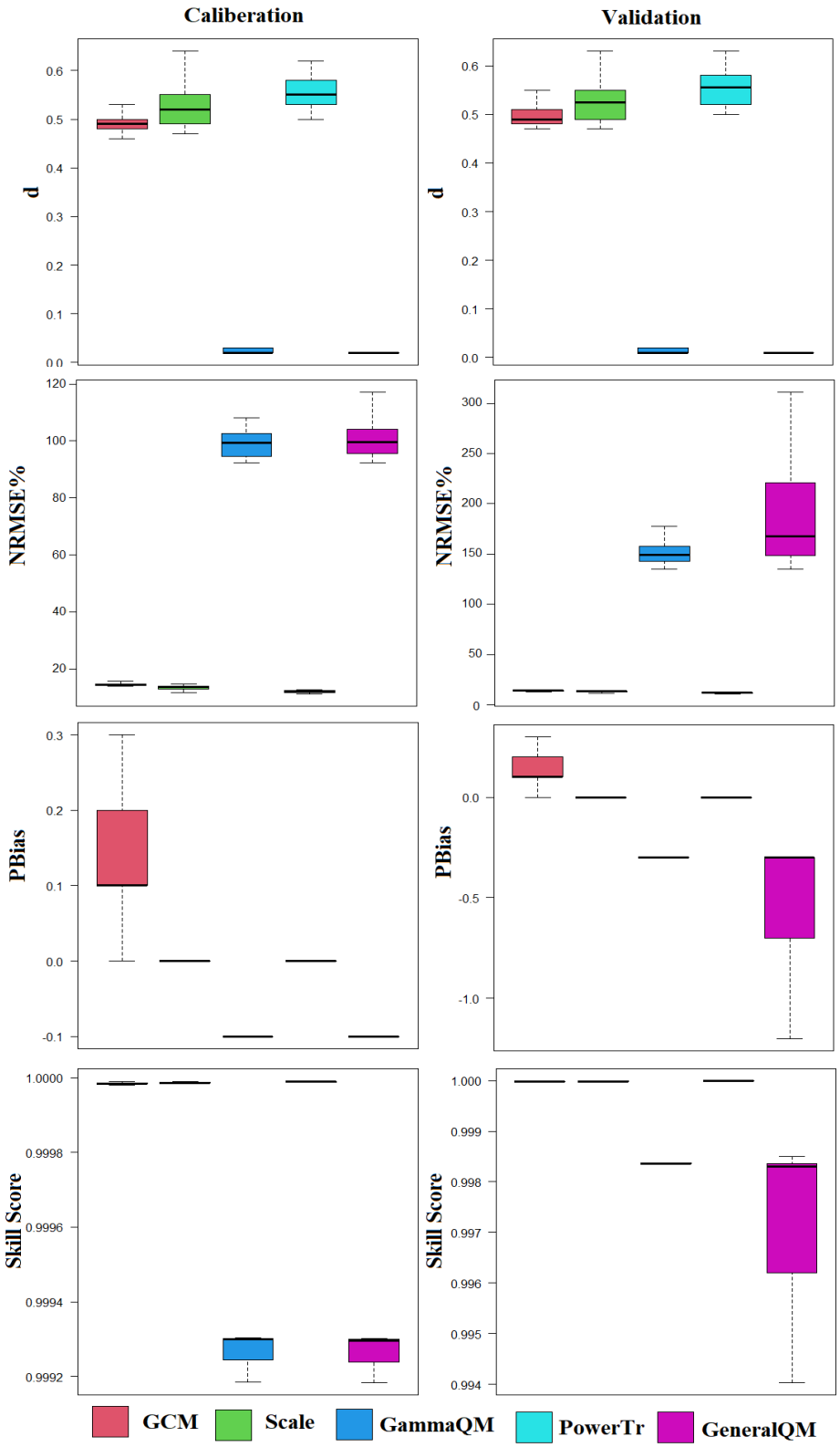

Figure S6. The statistical performance of the downscaled and raw MRI-ESM2 GCMs for maximum temperature.

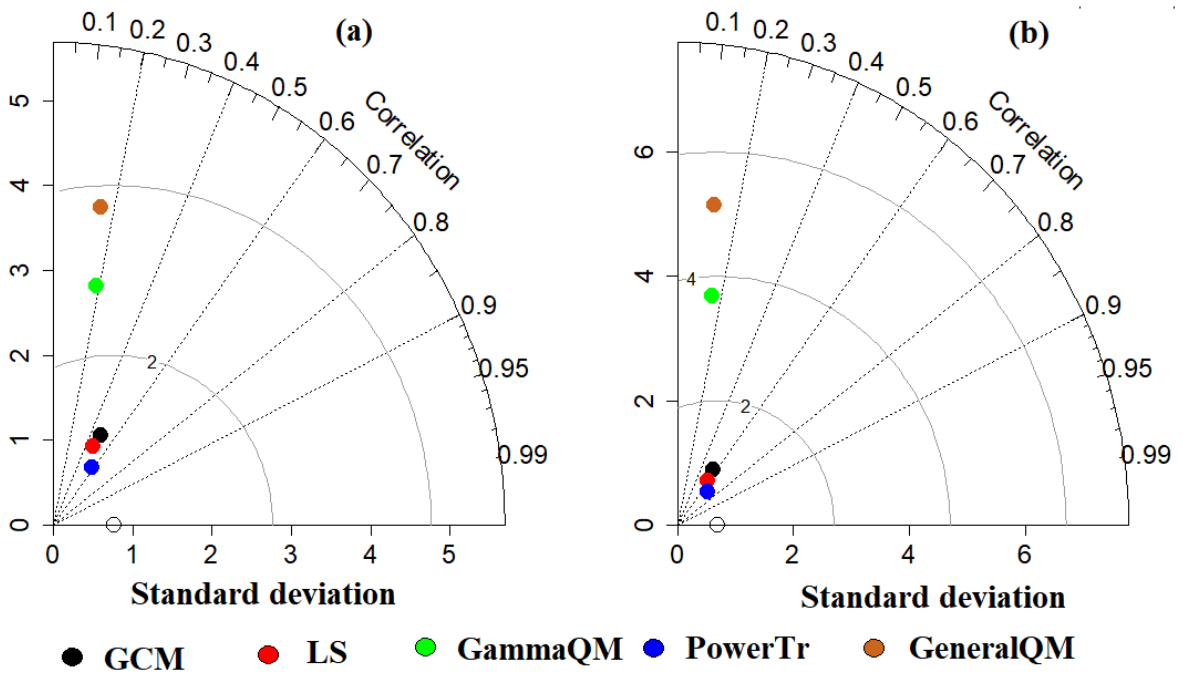

Figure S7. Taylor diagram shows bias correction methods' performance to correct EC-Earth-veg maximum temperature during **(a)** calibration; **(b)** validation periods.

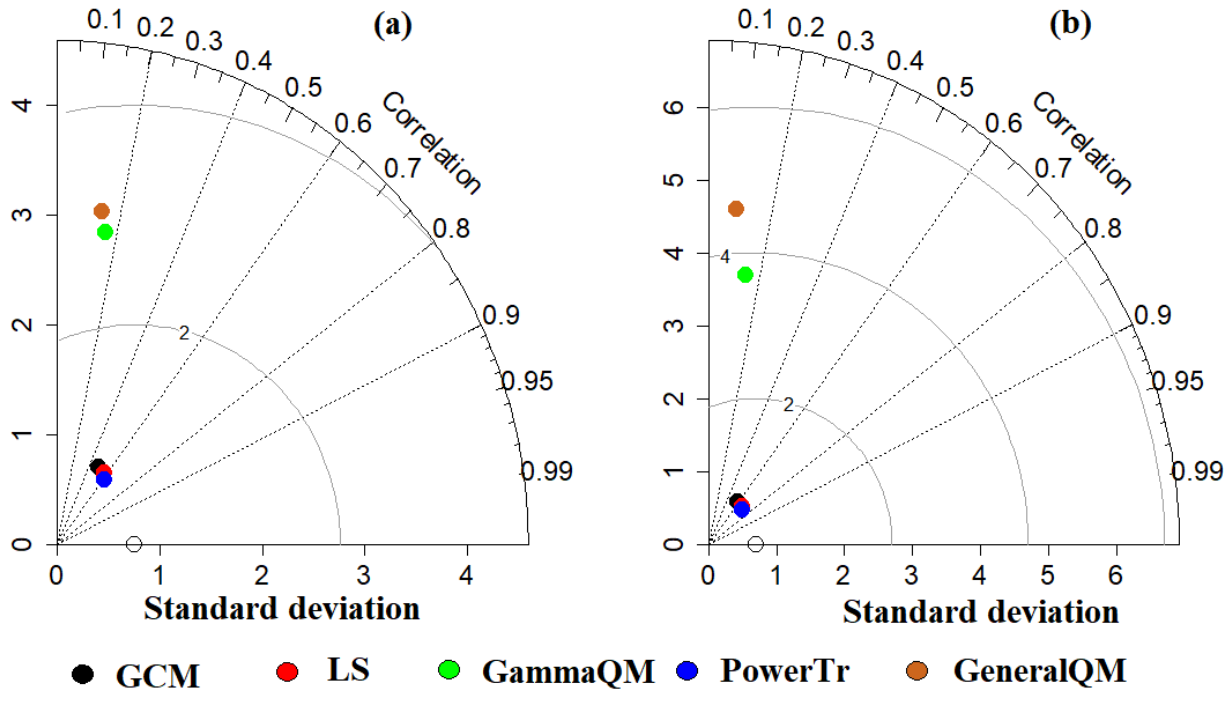

Figure S8. Taylor diagram shows bias correction methods' performance to correct MRI-ESM2 maximum temperature during **(a)** calibration; **(b)** validation periods

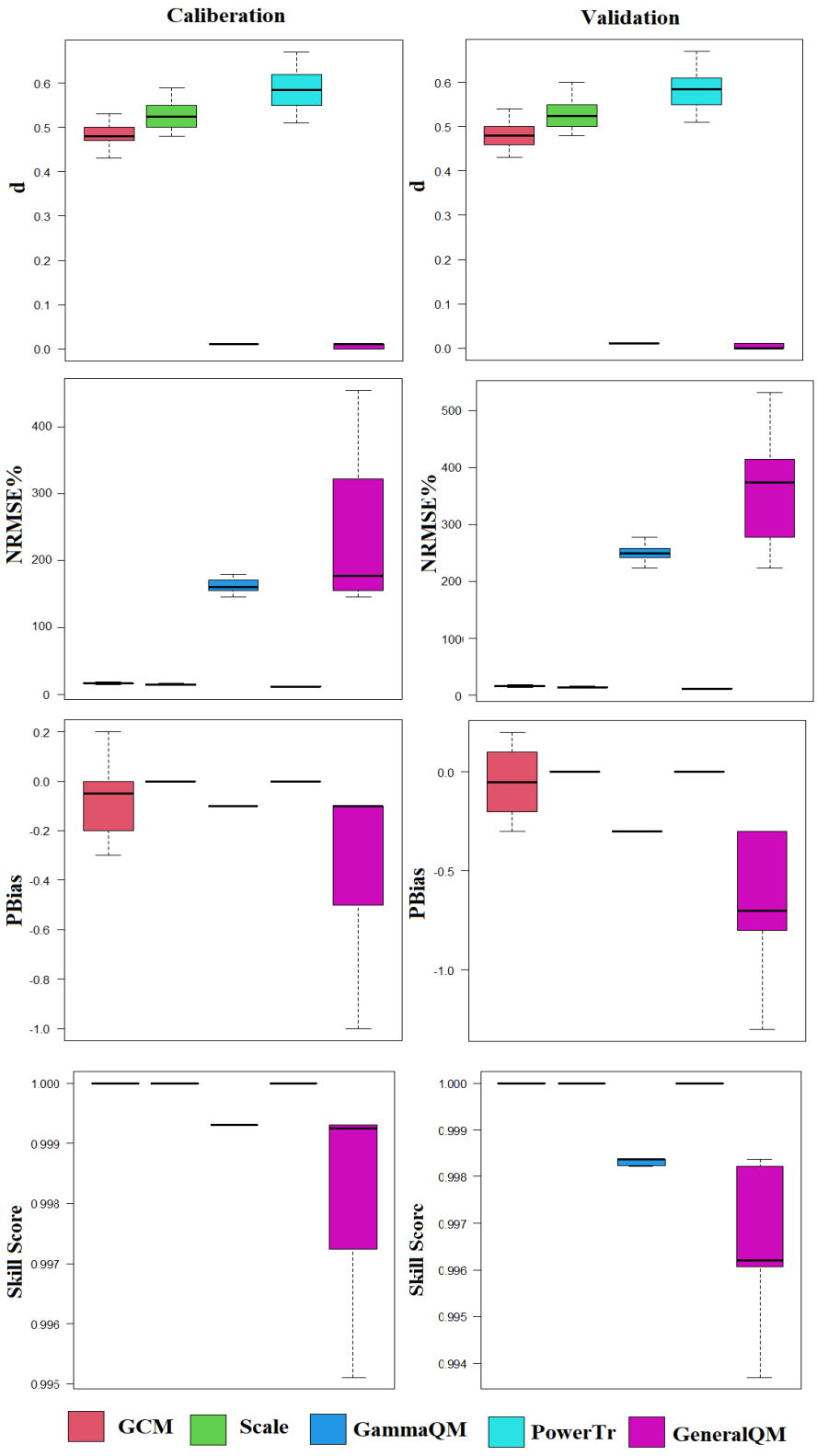

Figure S9. The statistical performance of the downscaled and raw EC-Earth-Veg GCMs for minimum temperature.

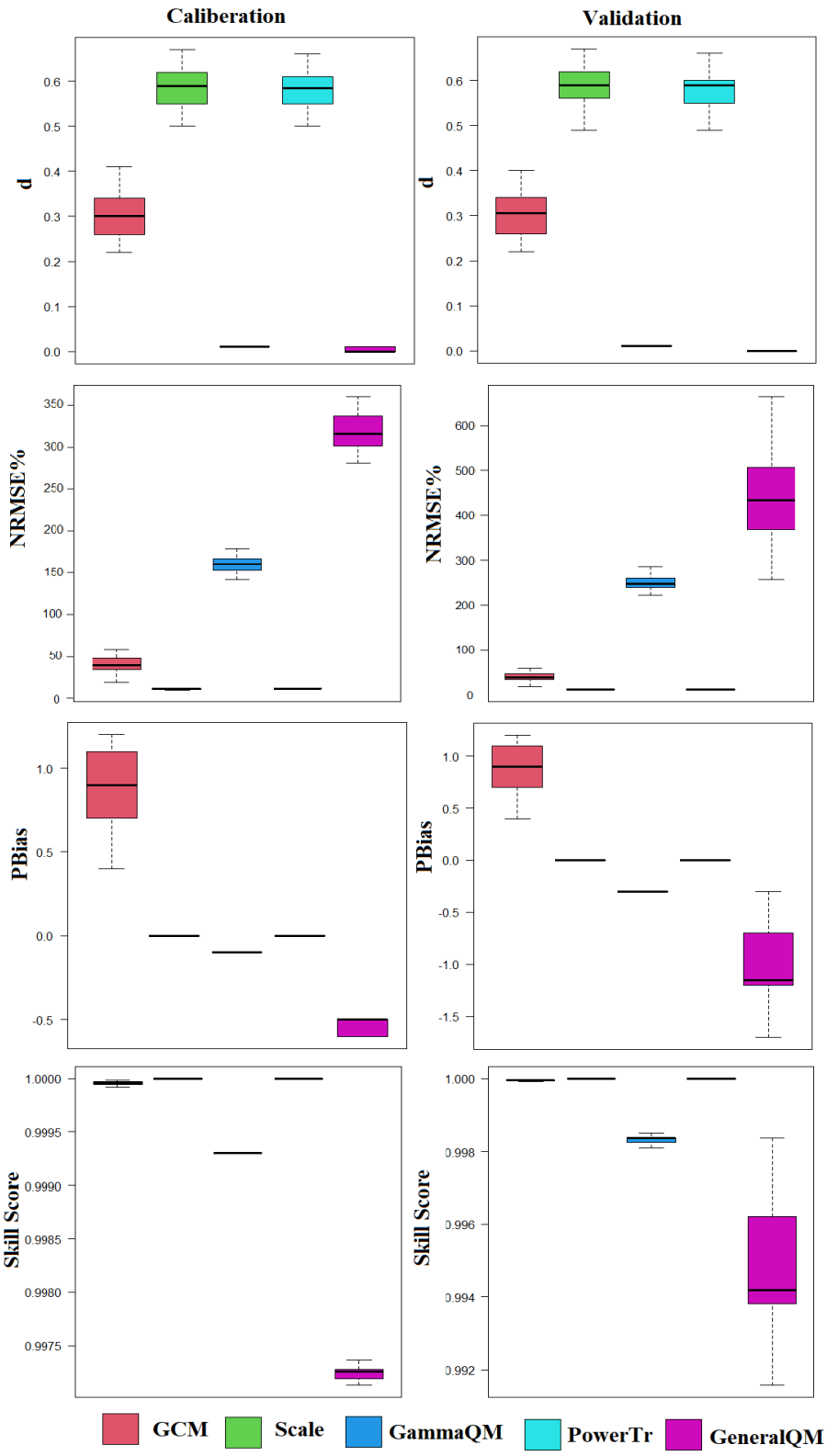

Figure S10. The statistical performance of the downscaled and raw MRI-ESM2 GCMs for minimum temperature.

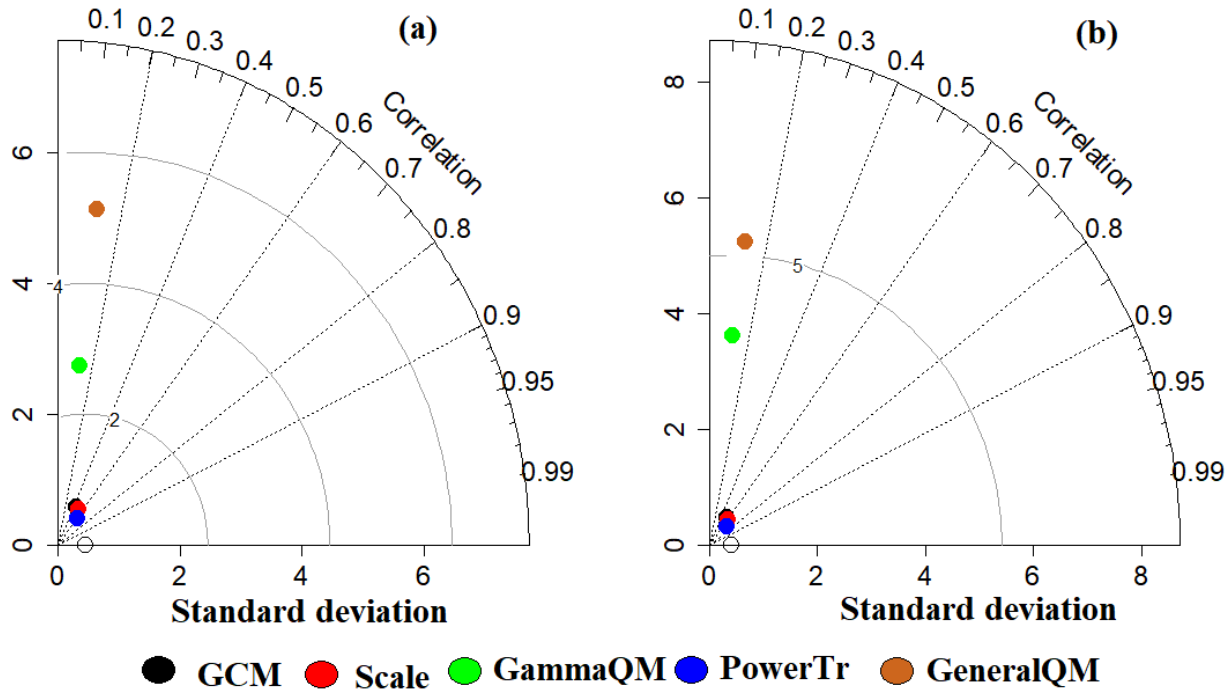

Figure S11. Taylor diagram shows bias correction methods' performance to correct EC-Earth-veg minimum temperature during **(a)** calibration; **(b)** validation periods

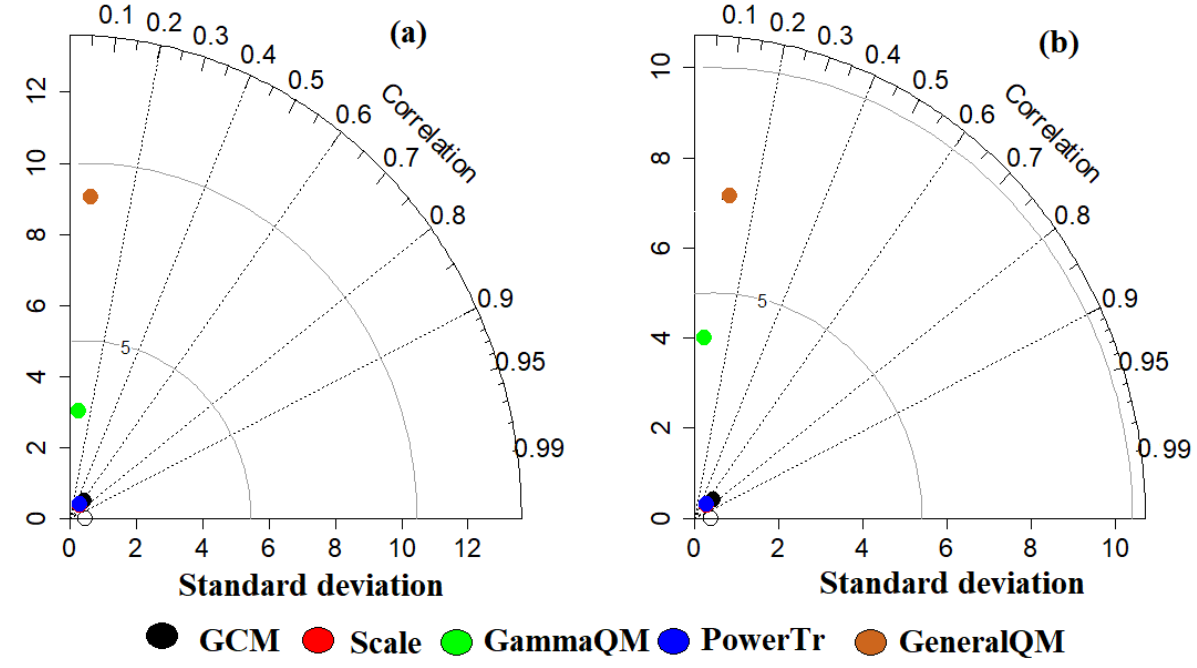

Figure S12. Taylor diagram shows bias correction methods' performance to correct MRI-ESM2 minimum temperature during **(a)** calibration; **(b)** validation periods